# Chapter 4

# Stellar Kinematics

**Abstract**

The He I 2.06 $\mu$m images presented in Section 3.2 indicate that the He I stars can serve as kinematic tracers in the CO-depleted central 1/4 pc. Radial velocities from the spectra presented in Section 3.3 are used to confirm gas and CO kinematics and extend them to the neighborhood of the central region. A new mass constraint of $\lesssim 1.8 \times 10^6\,M_\odot$ for this concentration is derived from these data in Haller *et al.* (1996). These velocities are compared with those derived independently by Krabbe *et al.* (1995). In light of the discrepancy, new spectral data are searched for high velocity stars in the central region.

## 4.1 Introduction

The mass distribution in the central parsec of the galaxy is critical to our understanding of the region and the processes which occur there. Of particular interest is whether or not a central dark massive component exists and its nature and extent. This is particularly critical as *HST* is providing evidence for central dark-mass concentrations in other galaxies which may be massive black holes similar to AGN engines. However, even with *HST/WFPC2* the spatial scales which can be probed in other nuclei are thus far insufficent to rule out more extended dark-mass distributions such as clusters of stellar remnants. In the GC, we may be able to place uniquely tight constraints on the extent of the central dark mass and test theories for the development of central massive black holes.

However, the GC introduces a number of obstacles which prevent a determination of the mass distribution limited only by spatial resolution. The CO-bearing stars, both discrete and as an integrated background population, are very effective at probing the kinematics from relatively large radii in to $\gtrsim 8''$. At that point, however, measurement and interpretation of CO based kinematics becomes significantly more ambiguous. First, the volume in question is too small to have a significant number of distinguishable, luminous, CO-bearing stars as would be required for a discrete analysis. Second, the velocity dispersion rises sufficiently to blur the sharp CO-band features as stars with different velocities contribute to the aggregate light. Third, there is a CO-depletion region in which the CO band depths become too shallow for kinematic use (Sellgren *et al.* 1987). This occurs either because the background population loses the CO in the stellar atmospheres through dissociation or mass stripping, or because the background stellar distribution does not peak as sharply as a more luminous, non-CO-bearing population, which dilutes the CO absorption with additional continuum. For these reasons, CO kinematic measures

become increasingly difficult in the very central regions. Further, interpretation of measured dispersions is not straight forward near this depletion region because the region's structure is ambiguous (cf. Haller *et al.* 1996). For example, if the CO depletion is caused by dilution by an additional, featureless population, then kinematics measured from the CO stars throughout the region can be interpreted as valid tracers of the kinematics. However, if the depletion is complete in a spherical region in which atmospheric CO is dissociated, perhaps by a strong central UV source, then CO-absorbing stars seen within this radius are projected from larger radii where the velocity dispersion is lower, resulting in a tendency to underestimate the enclosed mass. Extensive models of the behavior of the CO dispersion in these and other geometries and comparison with other cluster properties such as the light distribution allow Haller *et al.* (1996) to derive confidently enclosed mass measures in to $\sim 0.15$ pc. However, a kinematic sample which does not have these complications, such as the He I stars, is obviously useful as a check and to sample even closer to the center of the depletion region.

A second technique which has proven reliable at larger radii is to measure kinematics from the emission lines of the ambient gas. Similar kinematic measures can be derived all the way into the central region (e.g. Lacy *et al.* 1991). However, ionized gas is subject non-gravitational influences which are expected to distort its systematic motions in a region of strong magnetic fields (see review by Morris 1994) and energetic phenomena like the GC. For this reason alone, gas kinematics are unacceptable probes of the gravitational potential in the central parsec.

## 4.2 Kinematics from 1994 Data

### 4.2.1 Velocities and Positions

The data described in Section 3.3 were analyzed for radial velocities of He I emission-line stars. The data were already wavelength calibrated. For this experiment, a number of He I emission sources which were clearly stellar were extracted and their emission profiles fit to derive radial velocities which were subsequently corrected for heliocentric motion. A step which was more important for this analysis than for the study of the stellar population was determination of the location of the He I source relative to the dynamical center near Sgr A*. These locations were determined by comparing the spatial information present in the long-slit spectra with a high quality image of the region provide by M. Rieke. In an iterative fashion, starting from where observing notes, encoded telescope-mount coordinates, or a simultaneous guider image indicated the slit position was intended to be, a vector was extracted from a smoothed and rebinned copy of the image and compared with the spatial axis of the spectrum. For MMT data in which the slit passed near at least one bright source, this procedure gave positions repeatable to better than an arcsecond. Comparison of spectral features at derived slit intersections confirms the technique. For the Bok data with the coarser spatial scale and wider slit, an accuracy closer to $2''$ is achieved. In a few cases there were no high contrast sources and the slit location could not be definitively determined. With only one exception, these spectra did not have any stellar emission features and were probably well removed from the central cluster. These spectra will not be considered further. The one exception has two late-WN spectra which appear similar to spectra of a source near IRS 11 and AHH-NW which are available from other spectra, so it was redundant and not considered.

### 4.2.2 Systematic Biases

The velocities derived from the stellar emission lines are expected to be biased in two ways to a higher dispersion leading to an artifically high enclosed mass. The first bias is introduced by the winds in which this emission line is produced and the second by a selection effect to avoid confusion with ambient gas.

The He I 2.06 $\mu$m emission line is produced preferentially in a fast stellar wind (cf. Najarro *et al.* 1994). Correspondingly, the measured profiles are resolved and at least as broad as the expected velocity dispersion of the population. Through geometrical effects and increased error in profile fits, the measured velocities are expected to have more scatter than the intrinsic stellar velocities. We have endeavored to minimize the effect of this systematic bias in three ways. First, we have rejected from our kinematic sample those stars with He I 2.06 $\mu$m emission-line widths greater than 200 km s$^{-1}$ because stars with narrower profiles tend to give velocities measured from profile fits closer to their intrinsic velocities. Second, we have used the highest spectral resolution available to allow better profile sampling and more accurate fits and to distinguish stars with unacceptably wide emission lines. Third, we interpret the derived velocity dispersion as an **upper limit**.

The point of this experiment is to derive velocities of a population affected only by the gravitational potential and not by non-gravitational influences to which gas responds. Although Figure 3.1*a* indicates that most of the He I emission is associated with stars, the spectra in Chapter 3 also show a large amount of emission from ambient gas in the region with clear systematic motions. Hence, it is essential to distinguish stellar He I emission from gas emission to avoid contamination of the derived velocity dispersion by non-gravitational motions. Several steps were taken to avoid including gas velocities in Table 4.1. First, the spatial dimension available in the long-slit spectra allow us to select sources which are spatially unresolved and

Table 4.1: Measured Radial Velocties from He I Lines

| Source | Offset | FWHM [km/s] | $v_{lsr}$ [km/s] |
|---|---|---|---|
| IRS 16NW1 | $-1''$, $1''$ | 180 | $-196$ |
| IRS 16NW2 | $-1$, 1 | 320 | 433 |
| IRS 29 | $-2$, 1 | 250 | $-194$ |
| IRS 16NE | 3, 1 | 170 | 34 |
| GCHe5 | $-3$, 3 | 150 | $-26$ |
| GCHe3 | $-2$, $-5$ | 120 | $-239$ |
| IRS 13 | $-4$, $-2$ | 210 | $-153$ |
| IRS 34 | $-5$, 1 | 230 | $-174$ |
| between 10E & 16NE | 8, 5 | 150 | 34 |
| GCHe2 | 4, $-7$ | 220 | 180 |
| E of IRS 9 | 7, $-8$ | 150 | 132 |
| IRS 5 | 9, 10 | 150 | 85 |
| E of IRS 11 | $-10$, 12 | 180 | $-18$ |

brighter in emission than their surroundings. Second, we can use the image to check that an emission source is associated with a bright star. Third, we can reject sources with the same velocity as the surrounding gas. The latter was done both by comparing with spectra extracted from nearby positions and by comparing with published gas velocities derived from other emission lines. However, this latter selection criterion introduces a bias away from the local gas velocity. Again, we minimized the influence of this effect by maximizing the spatial and spectral resolutions to reduce confusion and by interpreting the derived velocity dispersion as an upper limit.

## 4.3 Comparison with Krabbe *et al.* (1995)

Contemporary to our observations, a number of other groups observed the central parsec (Libonate *et al.* 1995; Blum *et al.* 1995b; Eckart *et al.* 1995; Krabbe *et al.* 1995). One of these groups, Krabbe *et al.* (1995) (hereafter K95), had sufficient

coverage and spectral resolution to perform a kinematic analysis similar to that described in the previous section. A comparison of our observations and results is in order.

K95 used three different instruments. FAST, a Fabry-Perot imager, was also used by Krabbe *et al.* (1991). This instrument provides 0.9″ (undersampled) images of the central 30″ with a spectral resolution of 950. K95 observed only the He I 2.058 $\mu$m line with this instrument. With 18 images of 250 s each spaced at 150 km s$^{-1}$, these observations should have samped the He I profiles well. Unfortunately, they present a velocity-integrated, continuum-subtracted image rather than spectral profiles. This image agrees very well with Figure 3.1*a* with comparable spatial resolution. It includes the field north of IRS 16 but is not very deep and probably added useful kinematic information only for the strongest sources (IRS 16, 13, 15, AF, and AHH-NW).

CGS4 is a long-slit spectrometer with a 3.″1 wide slit and resolution 650–1310 used for $H$ and $K$. K95 list it as used for kinematics of IRS 7W, IRS 13E, IRS 15SW, IRS 15NE, IRS 9, and AF, but with this wide a slit, only the IRS 15, AF, and possibly IRS 13 observations are likely to be valid measurements. The IRS 7W and (mis-identified) IRS 9 emission sources are quite close to much brighter sources. A 3″ region around IRS 13 includes a tremendous amount of emitting gas at high velocities, but it is a very strong emission source so their data are probably dominated by the stellar emission.

3D is a very different instrument which is much more suited for these observations. All of the spectra K95 show are from this instrument and it contributed to most of their reported velocities. Hence, it is probably the most important instrument for this experiment. It is briefly described (Genzel *et al.* 1995) as an image slicing spectrometer which obtains 256 channel $K$-band spectra of a 16x16 grid of

$0\farcs52$ pixels with $\lambda/\Delta\lambda = 1000$ resolution on a NICMOS3 detector. Their net 45 minute exposure with $1''$ resolution has unique advantages. We review the most pertinent differences between this instrument and Fspec and compare their observations with our own.

First, K95 have complete two-dimensional coverage of the field in uniform conditions in contrast to our collection of disjoint long-slit spectra which individually have only one spatial axis. This allows them to know directly where each spectrum is in the field whereas we reconstruct the position as described above. In addition to allowing more precise determination of source positions, their data are preferred for distinguishing fine spatial features. They can, for example, compare the spectrum from a point with spectra of neighboring points in any direction. This is very valuable in the most crowded and gas contaminated regions. They can also peak up and extract a spectrum directly on a bright continuum source like IRS 13 whereas our slit positions were always off the centroid of this source and our spectrum of this source is therefore weaker and more contaminated.

Second, their data cover a longer wavlength range. They covered the entire $K$-band in each spectrum whereas Fspec in high-resolution mode provides $\approx 0.08\,\mu$m of coverage in one grating setting. Hence, they did not need to splice together spectra taken at different times with different grating settings with the inherent errors in registration this entails. Specifically, their data would be much preferred for determining line ratios such as Br $\gamma$/He $I_{2.06}$. Their coverage to longer wavelengths is not valuable in this study because these stars are relatively featureless in this region.

Third, for part of these observations they used a tip-tilt guider (ROGUE) with similar scientific advantages as FASTTRAC described in Section 3.2 (although with an optical guide star). In principle, this should have given them significantly higher

spatial resolution except that the $0\farcs52$ pixels clearly limit them to the net $1''$ resolution they report.

Fourth, in spite of the 45 minute on source integration they used for the central 8 arcsec$^2$ and reduced spectral resolution, our data have significantly higher S/N. Presumably this is because the slit spectrometer is more efficient than an image slicer. This is most evident in the spectra of the weaker sources which we have in commmon. Indeed, they even sum all of their candidate "WC9/Of" and He I stars to bring the signal out of the noise. Although this was clearly unnecessary for the He I stars as their IRS 13, IRS 16SW, and IRS 16NE spectra have strong features, it is the only way the He II, C III, and C IV features show. This reduced S/N is particularly significant in analyzing the stars with weaker emission features both for emission properties and for kinematics.

Fifth, our data have significantly higher spectral sampling, $50\,\mathrm{km\ s^{-1}\,pixel^{-1}}$ rather than $300\,\mathrm{km\ s^{-1}\,pixel^{-1}}$. As we have stresed in Section 3.5, this is essential in distinguishing the line widths and profiles to allow identification of WR, Oe, and narrow-line sources. As described in Section 4.2.2, high spectral resolution is valuable for kinematics for two reasons. First, a more precise fit to the line profile is possible with the better sampling; with a systemic velocity disperion of order $150\,\mathrm{km\ s^{-1}}$, a spectral resolution element significantly wider than this is a significant handicap. Second, the wide-lined stars are poor and biased kinematic probes and can not be distinguished from the preferred, narrow-lined probes. They have subtracted a systematic shift of $90\,\mathrm{km\ s^{-1}}$ from He I $2.058\,\mu$m velocities to compensate for P Cyg absorptions.

Despite these varied differences in the data sets, we are primarily in agreement. We see similar kinds of stars and identify mostly the same sources and our spectra of the same sources are in good agreement. Exceptions are that we do not detect

"WC9/Of" stars as they claim and we do not agree with their kinematic results. The former discrepancy could arise from our emphasis on the He I line or incomplete spatial coverage. The latter is in the direction predicted based on the biases described above and likely illustrates that their data is inappropriate for this analysis. However, missing a few high velocity stars due to incomplete spatial coverage, although unlikely to systematically affect our results (we did not **avoid** high velocity stars), could have a significant impact. To address these concerns, we carried out additional observations aimed at continuous spatial coverage of a portion of the field where the K95 data indicated a number of "WC9/Of" stars. In selecting a target region, we ignored the velocities reported by K95 in order to continue to have an appropriate unbiased kinematic sample.

## 4.4 New Spectroscopy to Search for High Velocity Stars

On the nights of April 11–13 1995, we returned to the MMT with Fspec in high-resolution mode and the infrared guider. Figure 4.1 illustrates the dense spatial coverage of the central cluster in the spectra obtained over the course of this project. Observational and data reduction procedures were the same as described in Section 3.3. Figure 4.2 shows some sample data after atmospheric, background, and dispersion correction. Despite the systematic spatial coverage, the data have no identifiable, unresolved sources with abnormally high velocities which would have a significant impact on the derived kinematics. A search of the data for significant C III or C IV lines revealed that there are no sources with these lines comparable in strength to the weaker He I sources discussed in this work.

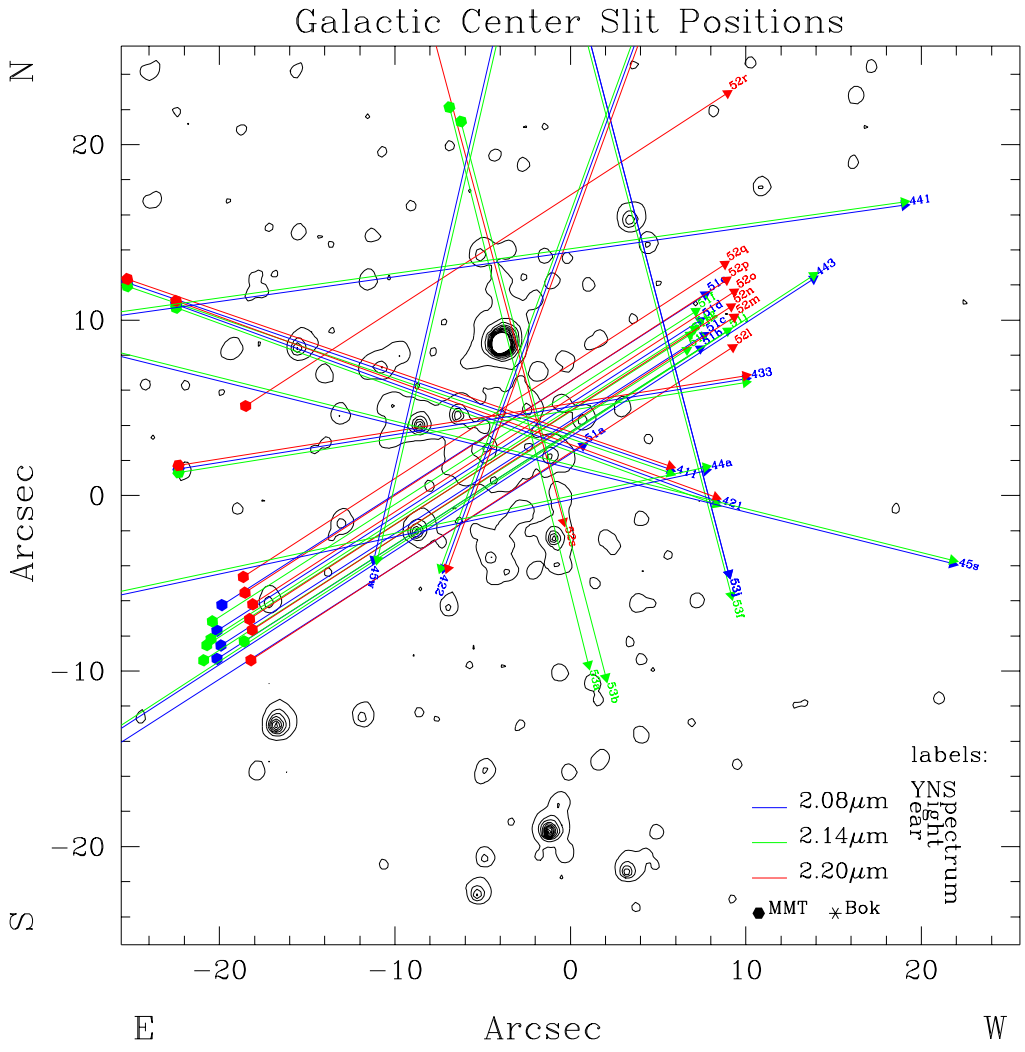


Figure 4.1: Confirmed Slit Locations, 1994–1995. This figure illustrates the fairly complete spatial sampling of the central cluster and shows where the slits were near various isolated sources. The background contours are of an image of the region provided by M. Rieke which was used to confirm the slit positions.

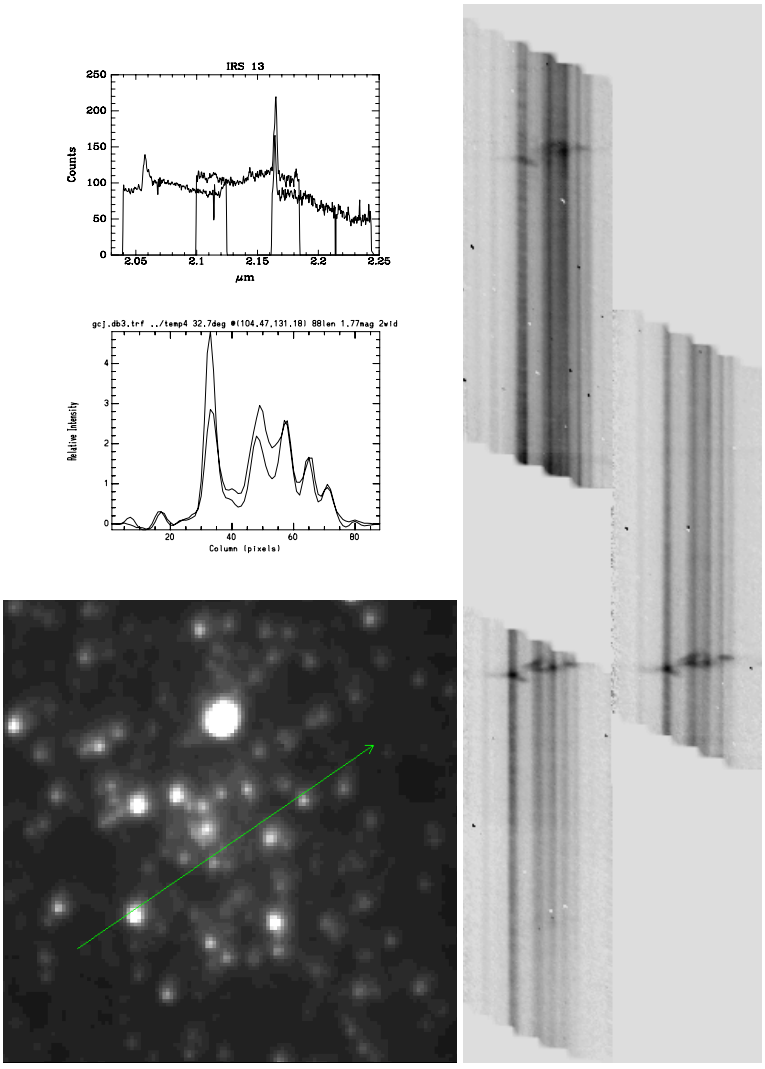


Figure 4.2: Sample Spectroscopic Data from the 1995 Observing Run. The image (courtesy M. Rieke) on the bottom left shows where the slit was located in the GC region for the three long-slit spectra on the right. IRS 7 is the brightest source in the image and IRS 9 is the bright source nearest the left end of the slit. The three spectra are of the same spatial location but with different grating settings. The top spectrum includes the He I 2.06 $\mu$m emission line, dominated by gas in this case. IRS 13's contribution can be seen above a white pixel defect. The middle spectrum is wavelength aligned and overlaps to cover the weaker He I 2.112 features which do not show well in the grayscale. The other prominent emission line is Br $\gamma$. The upper left panel shows a single column extraction from NE of IRS 13. Finally, the middle left panel compares the intensity distribution along the slit with a vector from the image after smoothing and rebinning. It allows one to identify the sources in the spectra, such as IRS 9.

## 4.5 Conclusions

The spectra described in Section 3.3 analyzed for radial velocities confirm and extend closer to the cluster center the kinematics derived from CO and gas observations. Data from all of these sources are combined with the light and CO distributions and detailed models (Haller *et al.* 1996) to derive a central dark component with mass 1–3.6$\times 10^6\,M_\odot$ which is possibly extended on a scale of 3 pc. This may be a massive central black hole or a collection of stellar remnants. The He I data are best interpreted as providing an upper limit on the enclosed mass due to systematic biases. The upper limit derived is substantially below that found by a similar analysis (K95). The datasets are compared and new MMT observations with Fspec densely sampling the central cluster do not indicate any overlooked high velocity He I sources or detectable C III/C IV sources.